Chapter 5
Energy Management of Maritime Grids Under Uncertainties

5.1 Introductions of Uncertainties in Maritime Grids

5.1.1 Different Types of Uncertainties

There are many types of uncertainties during the operation of maritime grids, i.e., demand-side uncertainties, generation-side uncertainties, and failure uncertainties, which are shown in Fig. 5.1.

Generally, navigation uncertainties are the main sources of demand-side uncertainties, such as the uncertain wave and wind and the adverse weather conditions. As we have illustrated in former Chap. 2, there are different management tasks of maritime grids, and the navigation uncertainties therefore can bring uncertainties to the demand, such as the propulsion load in ships and the corresponding calls-for-service delay for berthing.

For the propulsion load, conventional uncertain wave and wind will add navigation resistance and cause speed loss. To ensure the on-time rates, the power generation system requires a certain power reserve, noted as "sea margin" [1]. Table 5.1 shows the "sea margins" in the main navigation route around this world.

From the above table, the "sea margins" are generally within the range of "20%–30%", which represents a general ship design should at least have 30% power reserve [2]. This power reserve range has provided the flexibility for the maritime grids to accommodate navigation uncertainties towards economic and environmental objectives, and also gives the necessity of optimal energy management. When the navigation uncertainties continuously increasing, the route may become not suitable for navigation, and this type of navigation uncertainties is the "adverse weather conditions", the ships need to change another route for safety, which refers to the "weather routing" problems [3–5]. Additionally, navigation uncertainties will bring calls-for-service delays, which means the ships cannot arrive at the mission point at the scheduling time, and the service will be delayed. For example, the pre-scheduled

S. Fang and H. Wang, *Optimization-Based Energy Management for Multi-energy Maritime Grids*, Springer Series on Naval Architecture, Marine Engineering, Shipbuilding and Shipping 11, https://doi.org/10.1007/978-981-33-6734-0_5

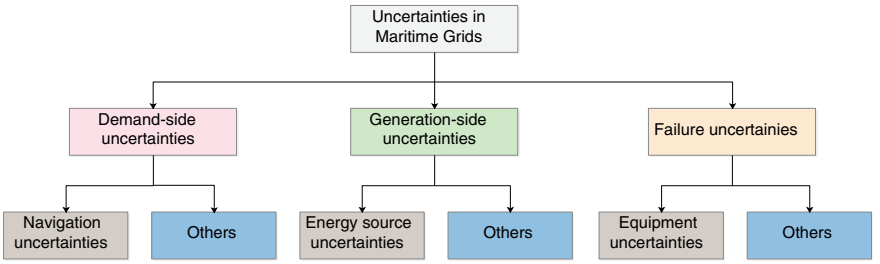

Fig. 5.1 Classification of uncertainties in maritime grids

Table 5.1 "Sea margins" for the main navigation route [2]

Navigation route	Sea margin
North Atlantic, heading west	25%–35%
North Atlantic, heading east	20%–25%
Europe-Australia	20%–25%
Europe-East Asia	20%–25%
Pacific	20%–30%

berth position for a delayed ship may stay idle state till the ship arrives, and the electric and logistic service will also be postponed, which brings uncertainties to the operation of the seaport.

The energy source uncertainties are the main sources of generation-side uncertainties. In conventional operating scenarios, the uncertainties of energy sources are quite limited since the main energy sources, such as diesel engines or gas turbines are highly controllable. However, in recent years, various types of renewable energy are integrated into maritime grids, and the inherent intermittency brings lots of operating uncertainties to the maritime grids, such as the photovoltaic energy in ships, and the offshore wind farms for island microgrid. Those types of uncertainties should be addressed to reduce the operating risks of maritime grids. Another type of energy source uncertainties is the main grid uncertainties from the uncertain electricity price and the main grid failures.

The equipment uncertainties generally include two types, the first one is for the failure and the second one is for the scheduled maintenance or replacement. Their difference is the failure occurs unexpectedly and the system needs to act for correction, and the scheduled uncertainties give much longer time for the system to re-schedule the operating plan.

The main classifications of uncertainties in maritime grids are illustrated above, and the uncertainties bring enormous operating risk to the maritime grids, and proper operating strategies should be promoted to mitigate their influence.

5.1.2 *Effects of Electrification for Uncertainties*

The above uncertainties have perplexed the maritime industry for a long time. For example, the adverse weather conditions have been viewed as one of the main reason for ocean accidents, for example, the accident of *Svendborg Maersk* in 2014 [6]. The equipment failures are also viewed as the enemy to the system reliability [7, 8]. Lots of control strategies have been studied to prevent their harmful effects, such as spare parts optimization [9] and system reconfiguration [8]. With the extensive electrification, the maritime grids become a highly coupled multi-energy system, and all the system resources can be used to mitigate one type of uncertainty. Here we give two examples to show the effects of electrification for uncertainties.

In conventional ships, the propulsion system is directly driven by the main engine by a gearbox, and the other onboard components are supplied by the shipboard power system, shown as Fig. 5.2.

The main engines cannot freely adjust their outputs, and only several gear positions can be selected, such as 1/2 full power or 1/3 full power. As a result, this type of adjustment is coarse and lacks flexibility for conventional navigation uncertainties, since, for most cases, the speed loss by navigation uncertainties is only 10%~15% of the total speed [2]. With extensive electrification, the propulsion system can be quickly responding to the navigation uncertainties due to the superior rotation regulation performance of electric machines [10, 11]. In this sense, the electrification can make ships navigate in a more steady speed range.

For conventional seaports, the logistic equipment consumes most of the energy consumption and they may be not driven by electricity, such as the rubber-tire gantry may be driven by diesel engines [12]. In some cases, the rest system may not consume all renewable energy integration. For example, the Jurong port of Singapore has 9.5 MW photovoltaic energy integration in 2016 [13], but some of them may be wasted in some time periods. However, with fully electrified, the maritime grids will have a larger capacity to accommodate the energy source uncertainties. Furthermore,

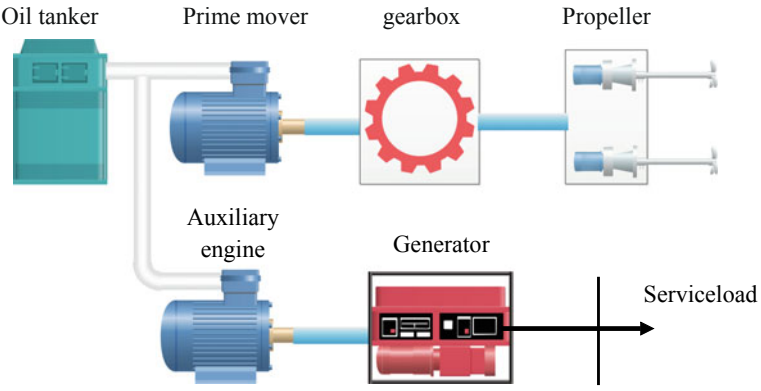

Fig. 5.2 Topology of conventional ships

the auxiliary equipment brought by electrification, such as batteries, combined heat-cooling power generators, can further enhance the reliability under main grid failures.

In summary, with full electrification, the maritime grids will have larger capacity and more resources to withstand different types of uncertainties, and with proper energy management, the economy, environment, and reliability objectives can be better achieved.

5.2 Navigation Uncertainties

5.2.1 Uncertain Wave and Wind

Generally in calm water, the propulsion load of ship has a cubic relationship with the cruising speed, shown as Fig. 5.3. The propulsion load will gradually increase with the speed and finally hits the "wave wall", and the maximum cruising speed achieves. When a ship sails on the sea, the wave and wind will add extra resistance and bring speed losses [2], and the wave wall will be moved to the left.

From Fig. 5.3, when considering the wave and wind, the cruising speed under the same propulsion load will decrease, and this refers to the "speed loss". To mitigate this speed loss, the main engine of ships should have adequate "sea margin", usually more than 15% by different navigation routes and seasons, as shown in Table 5.1. For example, in the route between Japan-Canada, the added resistance may scale up to 220% in some seasons, and the average is about 100% [14], and for most cases, the resistance in summer increases about 50%, and in winter, the resistance increases about 100% [14]. That added resistance will introduce more speed losses, and those speed losses may even accumulate and cause a severe delay in the destination. Therefore, energy management considering speed losses in uncertain wave and wind is essential for the maritime industry.

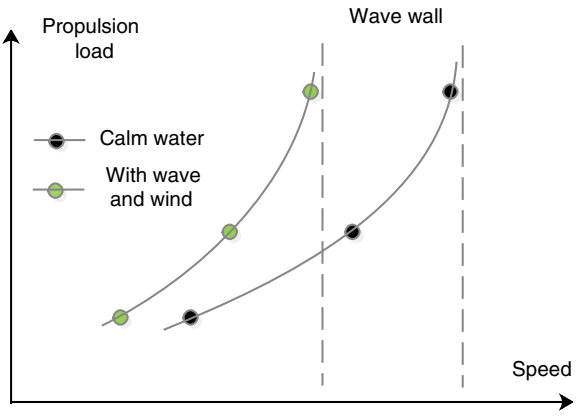

Fig. 5.3 Relationship between the propulsion load and the cruising speed

The performance of ships in wave and wind has been studied for a long time, and an empirical model is formulated in [15] by various CFD simulations, which are shown as follows.

$$R_t^T = R^C + \Delta R_t^{wave} + \Delta R_t^{wind} \tag{5.1}$$

$$\Delta R_t^{wave} = \frac{1}{\mathcal{L}} \cdot \rho_{water} \cdot g \cdot h_t^2 \cdot B_{int}^2 \cdot C^{D.wat}(\tau_t, \theta_t) \tag{5.2}$$

$$\Delta R_t^{wind} = \frac{1}{2} \cdot \rho_{air} \cdot S_{int} \cdot C^{D.air} \cdot \begin{bmatrix} \left(v_t^c + v_t^{wind} cos\theta_t\right)^2 \\ -\left(v_t^c\right)^2 \end{bmatrix} \tag{5.3}$$

$$v_t = \sqrt[c_2]{\frac{R^C}{R_t^T}} \cdot v_t^c \tag{5.4}$$

where R_t^T is the total resistance; R^C is the resistance of calm water; ΔR_t^{wave}, ΔR_t^{wind} are the added resistances of wave and wind; $\mathcal{L}$ is the ship length; ρ_{water} is the density of water; g is the acceleration of gravity; h_t is the wave height; B_{int} is the breath of ship intersection; $C^{D.wat}(\tau_t, \theta_t)$ is the added resistance coefficient, which is determined by wave-length τ_t and weather direction θ_t; ρ_{air} is the density of air; S_{int} is the area of ship intersection; $C^{D.air}$ is the air drag coefficient; v_t^{wind} is the wind speed; v_t^c and v_t are the cruising speed in calm water and wave/wind, respectively.

From the above Eqs. (5.1)–(5.4), there are four main decision variables to calculate the speed loss, i.e., wave height denoted as h_t, wavelength denoted as τ_t, wind speed v_t^{wind} and the weather direction θ_t. It should be noted that the weather direction is defined as the angle between the wind and the ship sailing direction. Since the wave has a similar direction with the wind, weather direction is used to indicate the influence of wave and wind.

Reference [15] has comprehensively studied the speed performance in wave and wind, and gives some fitting curves to calculate $C^{D.wat}$ under different weather direction (under B.N. 6), shown as Fig. 5.4. We can see this coefficient differs from each other when the weather direction changes.

With the above model, the speed loss under uncertain waves and wind can be predicted. Then in the energy management model, the speed loss can be considered in the voyage scheduling, and the propulsion system can response to the speed loss and ensures the punctuality of the ship's navigation.

5.2.2 Adverse Weather Conditions

Adverse weather conditions are those scenarios or areas which are not suitable for navigation [16, 17], and the ships should avoid this type of area for safety. Adverse

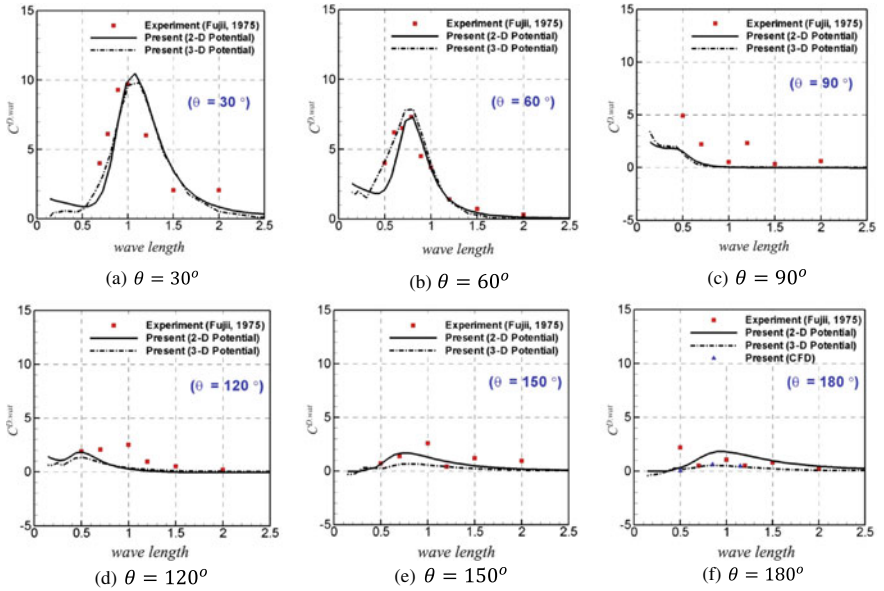

(a) $\theta = 30^o$ (b) $\theta = 60^o$ (c) $\theta = 90^o$

(d) $\theta = 120^o$ (e) $\theta = 150^o$ (f) $\theta = 180^o$

Fig. 5.4 Fitting curves to calculate added resistance of wave. Reprinted from [15], with permission from Elsevier

weather conditions generally include the typhoon or strong ocean current and the following Fig. 5.5 shows the influence of adverse weather conditions on the ship's navigation.

In Fig. 5.5, the primary navigation route is from Singapore to Inchon. The red dash line is the conventional navigation route from Singapore to Inchon due to the shortest distance. However, under pre-voyage weather forecasting, this navigation route is under the influence of a typhoon. Based on this information, the first stage chooses another navigation route (blue dash line) to keep away from the typhoon. In real-time navigation (second stage), the forecasting trajectory of typhoons may change to the black line, and the navigation route obtained in the first stage may still under the influences of typhoons. In this case, the second stage will modify the navigation route and the corresponding cruising speeds as the purple dash line for safe sailing.

From above, the uncertainties of adverse weather conditions come from the weather forecasting error, and the navigation route changes led by the adverse weather conditions will have different energy requirements on the ship power system.

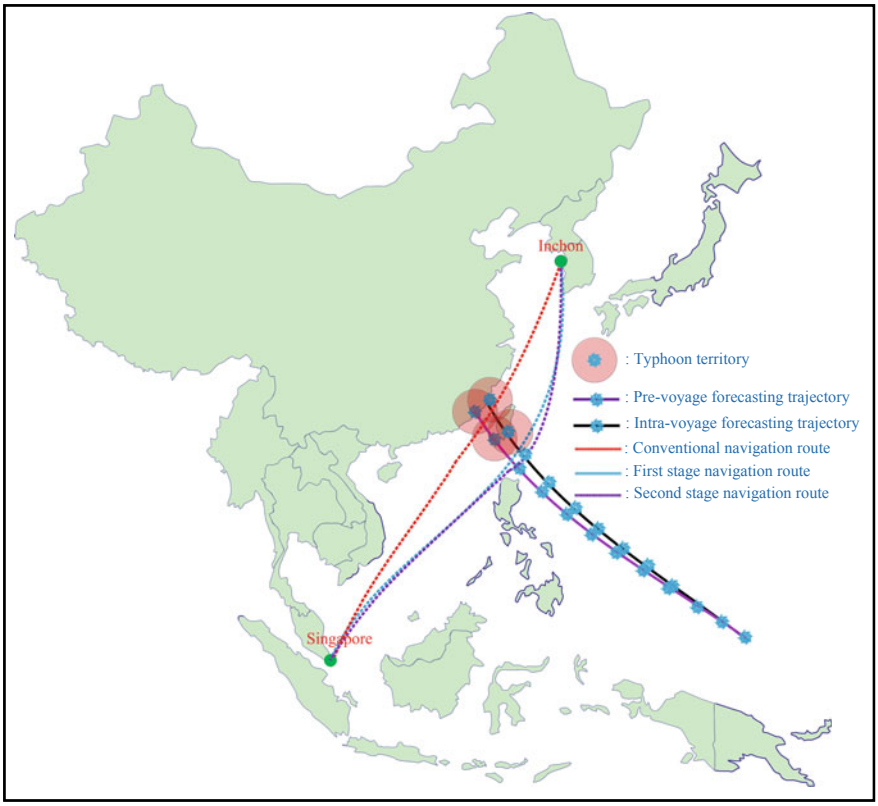

Fig. 5.5 Adverse weather conditions and the two-stage adjustment

5.2.3 Calls-for-Service Uncertainties

The former two types of uncertainties mainly influence the operation of ships and will bring delays to the destination, which brings calls-for service uncertainties to the seaport or other service facilities, such as islands or ocean platforms.

Generally, the services provided to the ships are classified as (1) the logistic services, i.e., cargo handling, and (2) the electric service, i.e., cold-ironing. Since the ships may not arrive on time for different reasons, as stated above, all the services may be delayed. Figure 5.6 shows the influences of calls-for-service uncertainties.

From above, the calls-for-service delays led to different power demand curves, which require different energy schemes. There are two main types of power demand changes, i.e., service delay and service accumulation. The service delay will not change the shape of power demand but only delays them, like the cold ironing power. The other type is the service accumulation, like cargo handling. This type of service has a constant total service workload, and if the service is delayed and the service will accumulate to increase the maximal power demand.

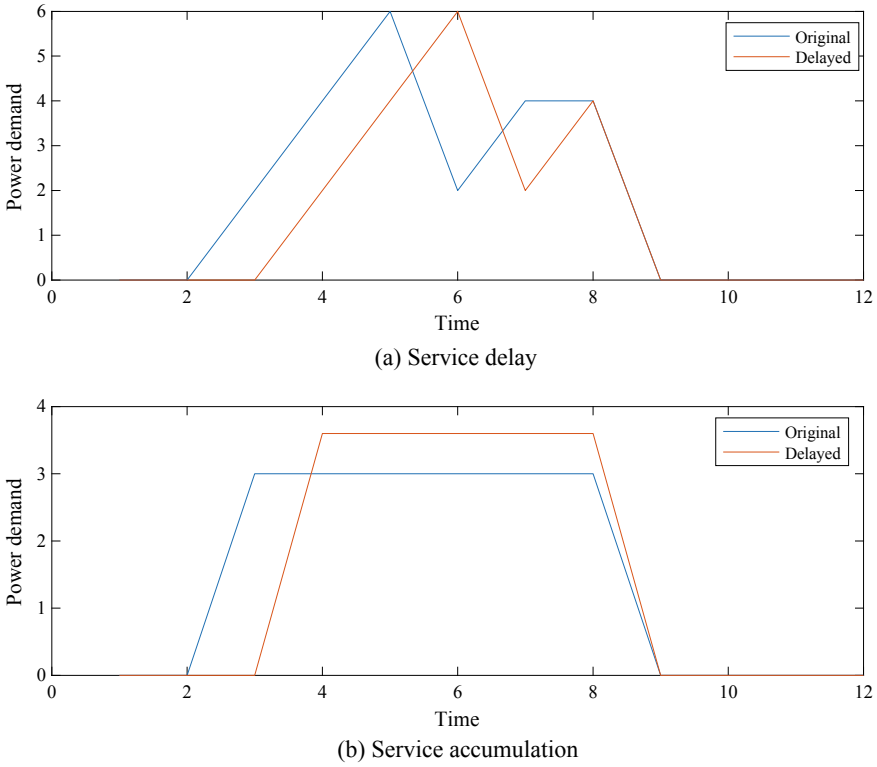

(a) Service delay

(b) Service accumulation

Fig. 5.6 Influences of calls-for-service

5.3 Energy Source Uncertainties

5.3.1 Renewable Energy Uncertainties

Nowadays, environmental issues have been the major concern from the globe, and renewable energy is gradually widely spread in the maritime grids, as we have stated in Chap. 1. However, renewable energy generally has high intermittency and a specified energy management method should accommodate this uncertainty. The following Fig. 5.7 gives a typical wind speed pattern.

The wind speed pattern can be depicted as a spectrum, and a high value indicates a high variation in that timescale [18]. In Fig. 5.7, the first peak is in the timescale of minutes, and the sites with high average wind speed tend to have a lower peak. This variation, referred to as the short-term variation, has been mitigated by many control strategies [19–21]. In the timescale of more than one day (Macro-meteorological range), there are three peaks, (1) Diurnal pattern, or named as the day-night pattern, which is led by the temperature difference between day and night; (2) depressions

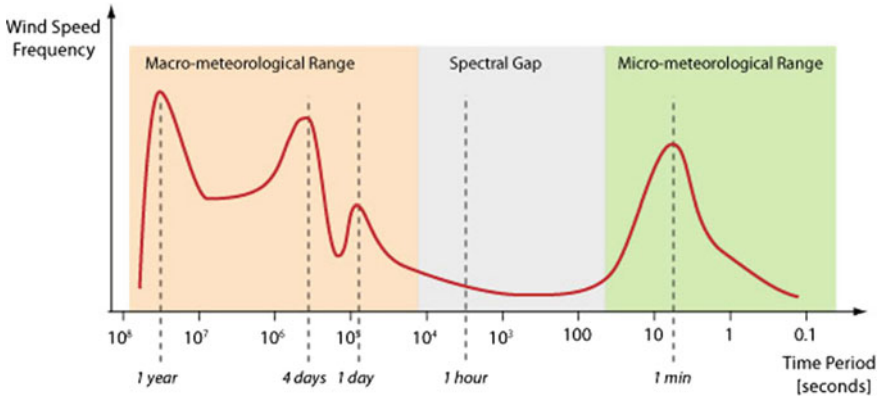

Fig. 5.7 Wind speed patterns. Reprinted from [18], open access

and anti-cyclones, and this phenomenon is more distinct in oceanic than continental regions.; (3) annual pattern, varies with the degree of latitude and vanishes close to the equator. In the following Fig. 5.8a, b, the power outputs of different wind turbines in a day and different seasons are shown.

From the above figure, we can see significant variations by different wind turbines and different seasons. As for the photovoltaic energy, the variations by different modules and different seasons are shown in the following Fig. 5.9a, b.

As above, the power outputs of the wind farm and photovoltaic farm are highly fluctuating, and even after deliberate forecasting, the error is still inevitable. Table 5.2 gives the forecasting error of renewable energy through various methods. The root-mean-square error (RMSE) are around 1–5%, which should be considered in the energy management of maritime grids.

5.3.2 Main Grid Uncertainties

The maritime grids can be mainly operated in (1) grid-connected mode; and (2) isolated mode. Two modes are shiftable for most of the maritime grids. For example, the ships are in isolated mode when sailing, and are in grid-connected mode when receiving the cold-ironing power from the seaport. For a seaport, it can also operate in isolated mode when having enough generators or renewable energy integration.

When in grid-connected mode, the main grid is generally the main energy source of maritime grids. However, there will be many uncertain failures that happened in the main grid and even cause a loss of power. The maritime grids generally don't have a strong network structure, and therefore an energy management method with considering the main grid failure is essential for the safety of maritime grids [26].

Besides, the main grid and the maritime grid maybe not under the same administrator, and the maritime grid should purchase electricity from the main grid, and

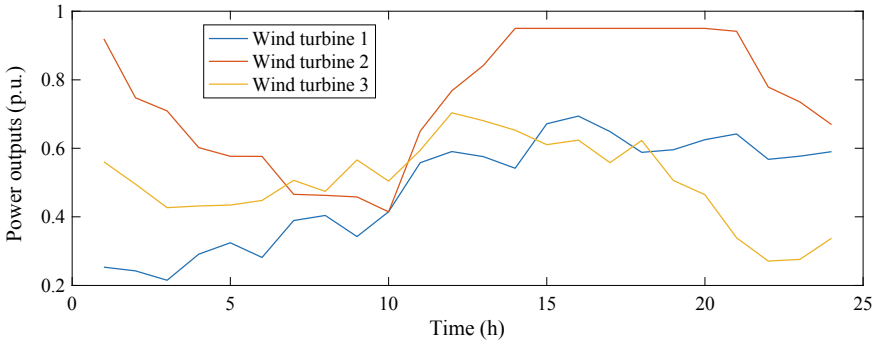

(a) Power outputs by different wind turbines

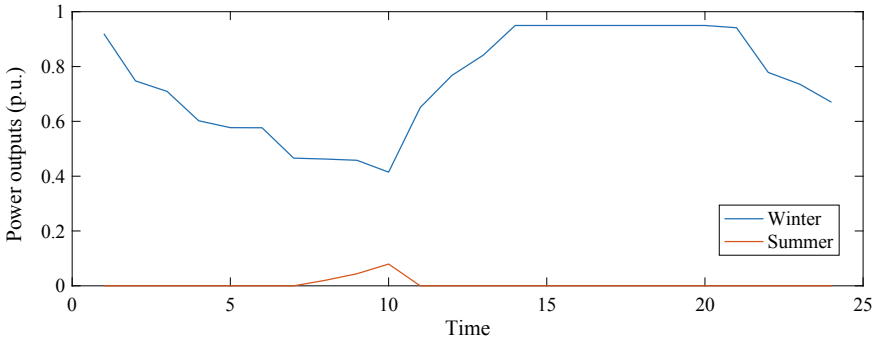

(b) Power outputs in different seasons

Fig. 5.8 Power outputs of different wind turbines and in different seasons

the electricity prices also have uncertainties. The maritime grid should aggregate the total power demand and negotiate the price with the main grid. The price may change in every round of negotiation [27], which also brings the main grid uncertainties.

5.3.3 Equipment Uncertainties

The equipment uncertainties in maritime grids come from two aspects: (1) the equipment failure; and (2) the scheduled maintenance. Their difference is the equipment failure may happen unattended but the latter one is planned.

For the equipment failure, the energy management system of maritime grids has to make enough power reserve for each severe scenario [8]. In [28, 29], to avoid the influence of the onboard generator's failure, the generation system have reserved a certain part of capacity, which are the same in ships and seaports. For a seaport,

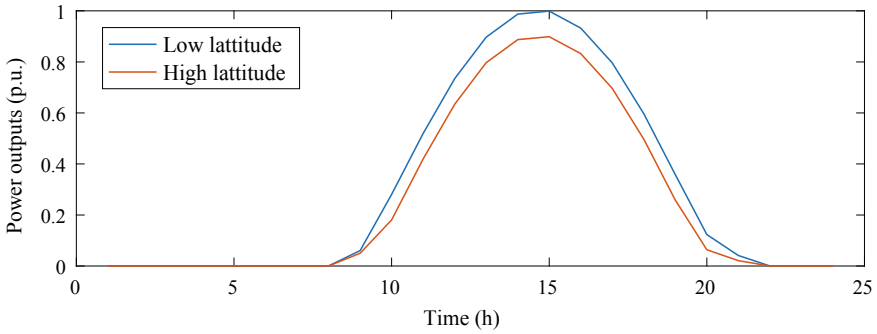

(a) Power outputs in different lattitude

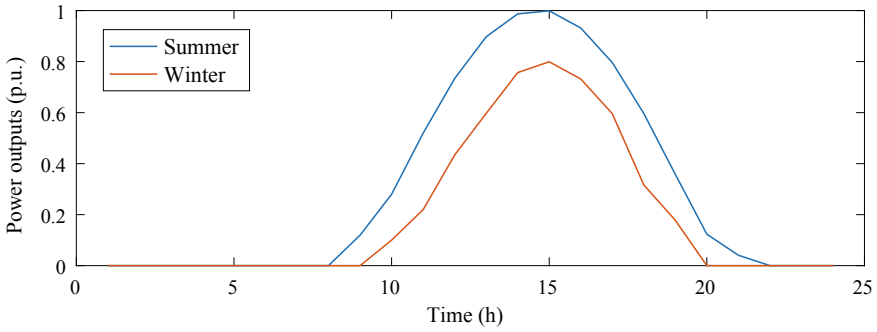

(b) Power outputs in different seasons

Fig. 5.9 Power outputs of different photovoltaic modules and in different seasons

Table 5.2 Forecasting error by different methods

Methods	Renewable energy	Timescale	Error (%)	References
f-ARIMA	Wind	Day-ahead	5.35	[22]
ANN	Wind	Day-ahead	1.32–1.56	[23]
SVM	PV	120 h	1.21	[24]
ARIMA	PV	1~39 h	21	[25]

the power reserve ratio can be lower since the main grid can provide enough power with high reliability, but the within generators still need to be standby for uncertain failure.

For the scheduled maintenance, the equipment out of service is known in advance, and the energy management system can make necessary adjustments. For example, when a generator in a seaport is planned to be in maintenance, the administrator of the seaport will give a new energy plan to the upper main grid to purchase more electricity [27].

5.4 Data-Driven Optimization with Uncertainties

5.4.1 General Model

The main types of uncertainties in the operation of maritime grids are illustrated as above. To ensure the safety and reliability of maritime grids, considering the above uncertainties in energy management is necessary. Nowadays, stochastic optimization [30–32] and robust optimization [32–34] are two main types to address the uncertainties, which are shown as following Eqs. (5.5) and (5.6), respectively.

$$\min_{x \in X} g(x) + E\left(\min_{y \in Y(x,\xi)} f(y)\right) \tag{5.5}$$

$$\min_{x \in X} g(x) + \max_{\xi \in U}\left(\min_{y \in Y(x,\xi)} f(y)\right) \tag{5.6}$$

In stochastic optimization (Eq. (5.5)), x is the first stage decision variables which are not determined by uncertainties; X is the feasible region of x; $g(x)$ is the objective function of the first stage; ξ is the uncertain variables, and $Y(x, \xi)$ is the feasible region of y determined by x and ξ; $f(y)$ is the objective function of the second stage; $E(\cdot)$ is the expectation. In this model, the uncertain variable ξ is depicted by the probability distribution, such as the probability distribution of equipment failure, or the probability distribution of renewable energy output, and so on. Then stochastic optimization seeks the optimal solution within the feasible region defined by the probability distributions.

In robust optimization (Eq. (5.6)), the main difference is the uncertain variable ξ is described by the uncertainty set U, including the upper/lower limits and the uncertainty budget, which mainly has polyhedral models [35] and ellipsoid models [36]. Then robust optimization seeks the optimal solution in the worst case in the defined uncertainty set and brings conservatism. With above, the primary problem of the uncertainty modeling is how to determine the feasible regions, such as the probability distributions in stochastic optimization and the uncertainty set in robust optimization.

As above, how to get the range of uncertain variables, i.e., the probability distribution function or the uncertainty set of ξ, is the basic problem of the optimization model. Nowadays, with the development of measurement and communication technology, more operating data can be transmitted and stored in the control center in real-time. How to use this type of massive data to model the feasible region of uncertainty has become a hot topic, and various methods have been proposed.

5.4.2 Data-Driven Stochastic Modeling

Stochastic modeling is to get the probability distribution functions of uncertain variables, and there are three types in general, (1) the non-parametric probability modeling; and (2) stochastic process modeling and (3) artificial intelligence methods.

The non-parametric probability modeling method directly extracts features from the original dataset and doesn't limit the probabilistic distribution prototype [37], thus may have higher accuracy when having limited knowledge on the dataset characteristics. Based on the diffusion-based density method, [38] proposes a non-parametric probabilistic model for wind speed. Later on, [39] proposes a model for wind speed combined the non-parametric probability modeling and auto-regression modeling. Then based on the non-parametric probability modeling, [40] formulates a probabilistic optimal economy dispatch model for a renewable integrated microgrid, and the case study proves the proposed method can improve the economic behaviors during uncertainties.

The basic idea of stochastic process modeling is to use a series of simple kernel functions to fit the complex function [41]. Based on different basis functions, stochastic process modeling has many representatives. The autoregression and moving average (ARMA) method is one of them and has been utilized in renewable power prediction, and power demand prediction [22, 25]. To reduce the dimension of the dataset, many reduction algorithms are implemented. Based on Karhunen-Loeve expansion, a time-space modeling method for renewable energy is proposed in [42, 43]. Then [44] proposes a solution method for this uncertainty modeling, and shows a lower computational burden with acceptable accuracy.

Compared with the above two types, the methods based on artificial intelligence has stronger data mining ability. The uncertain set can be directly modeled and no necessary to follow the conventional process of "probability distribution formulation-sampling-scenario reduction". Until now, various methods, such as the generative adversarial network (GAN) [45], recurrent neural network (RNN) [46], extreme learning machine (ELM) [47], are implemented to provide uncertain set by massive original dataset.

5.4.3 Data-Driven Robust Modeling

Robust modeling is to get the set of uncertain variables, and there are also three types in general, (1) the polyhedral set; and (2) the ellipsoid set and (3) the uncertain set based on scenarios.

The polyhedral set is the most commonly used uncertainty set for robust modeling, which is based on a series of upper and lower limits, shown as Eq. (5.7).

$$U = \left\{ \xi_t | \underline{\xi} \leq \xi_t \leq \bar{\xi}, \forall t \in T \right\} \tag{5.7}$$

where $\underline{\xi}$ and $\bar{\xi}$ are the lower and upper limits of ξ_t. If the uncertainty series follows the Markov law, the lower and upper limits may become $\underline{\xi} = \underline{\xi}_t(\xi_{t-1})$ and $\bar{\xi} = \bar{\xi}_t(\xi_{t-1})$. To limit the range of uncertain variables, uncertainty budget constraints may be added, shown as Eq. (5.8).

$$\underline{\eta} \leq \sum\nolimits_t \xi_t \Big/ \mu \cdot |T| \leq \bar{\eta} \tag{5.8}$$

where μ is the expectation of ξ; and $\underline{\eta}$, $\bar{\eta}$ are the lower and upper budgets of uncertain variable ξ. The uncertainty budget is used to limit the dramatic changes and reduce the conservatism of the robust model.

The second type is the ellipsoid set, which aims to solve the inconsistent characteristic at the boundary of the uncertain set. A general form is shown in Eqn.

$$U = \left\{ \xi_t \middle| (\xi - \mu)^T \cdot \sum\nolimits^{-1} (\xi - \mu) \leq \Gamma \right\} \tag{5.9}$$

where μ is the expectation of ξ; and $\sum$ is the correlation matrix of ξ. Li et al. [48] use the ellipsoid set to model the uncertainties, and find the ellipsoid set can better represent the uncertainty when approaching the boundary. Kumar and Yildirim [49] proposes the minimum volume enclosing ellipsoid (MVEE) method to limit the uncertainty in the smallest ellipsoid and reduce the conservatism. Based on MVEE, [50] studies the robust optimization based on the ellipsoid set, and proposes an invalid constraint reduction method to simplify the solution method.

Besides the above two modeling methods, there is a modeling method based on extreme conditions. In [51], an ellipsoid set of uncertainty is first formulated and then several extreme points are selected to form a convex set. The formulated robust model is shown as follows.

$$\begin{cases} \max\limits_{\xi_n \in U_n} \left(\min\limits_{x, y_n} f(x, y_n, \xi_n) \right) \\ s.t. A(x, y_n, \xi_n) = 0 n = 1, 2, \ldots, N \\ B(x, y_n, \xi_n) \leq 0 n = 1, 2, \ldots, N \end{cases} \tag{5.10}$$

where ξ_n is the uncertain variable in the n-th extreme scenarios, and y_n is the corresponding second stage decision variables; A and B are the equality and inequality constraints, respectively.

Another robust modeling formulates the uncertain set as a convex envelope to contain all the pre-given extreme points and can be shown as Eq. (5.11). α_n is the ratio for the n-th extreme scenario.

$$U = \left\{ \xi | \xi = \sum_n \alpha_n \cdot \xi_n, \sum_n \alpha_n = 1, \alpha_n \geq 0 \right\} \tag{5.11}$$

5.5 Typical Problems

5.5.1 *Energy Management for Photovoltaic (PV) Uncertainties in AES*

As the main representative of maritime grids, AESs face many uncertainties during navigation. This Chapter focuses on the uncertainties of onboard photovoltaic (PV) integration. This research is illustrated in detail in [52].

(1) Onboard PV power forecasting

In land-based PV power forecasting, the PV power is determined by three factors, i.e., the irradiation density, denoted as I^{Gh}, and the angle between solar rays and the PV modules, denoted as θ, and the generation efficiency, usually determined by the ambient temperature [53], denoted as η^{PV}. However, some differences compared with the load-based applications should be incorporated into the onboard PV forecasting.

The first difference is that the ship will constantly move along the navigation route. As shown in Fig. 5.10, the ship has different locations when t_1 and t_2, meanwhile the direction of solar rays, as well as the ambient temperature along the navigation route, are also changed. Therefore, it is sensible to utilize the measured data along the route, rather than the data in a stationary place to predict the PV generation.

The second difference is that the shipboard deck will constantly swing when cruising and change the angle between solar rays and the PV modules [53], shown in Fig. 5.11. The angles between solar rays and ship decks become $(\theta \pm \phi)$, which further affects the PV generation outputs. In general, the swinging direction of ships

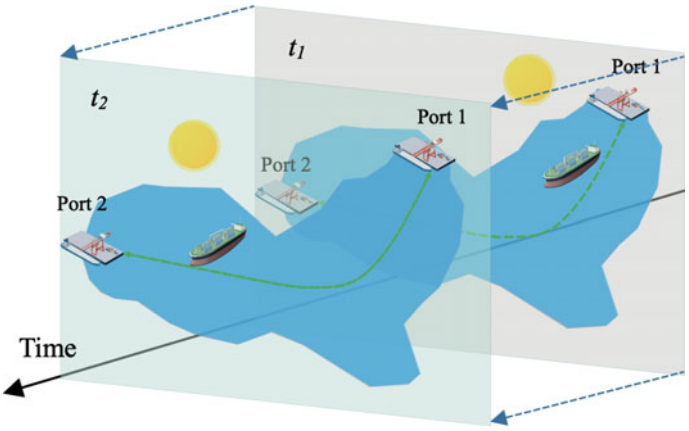

Fig. 5.10 An illustration on the moving of ships

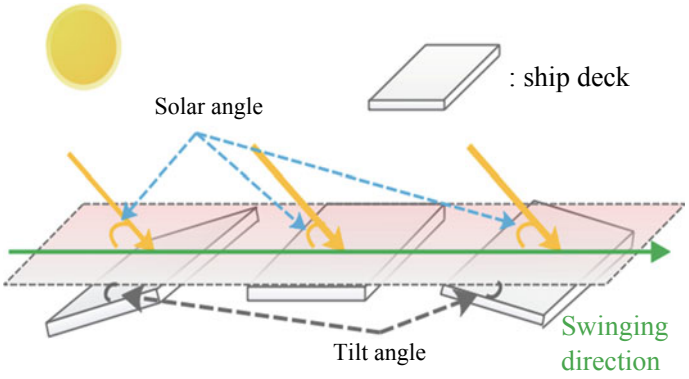

Fig. 5.11 Definition of the angle of solar ray and the tilt angle. Reprinted from [52], with permission from IEEE

is the same with the wind direction and the tilt angle is determined by the wind speed. So, it is necessary to incorporate wind speed along the navigation route to forecast the tilt angle range of ships.

(2) Two-stage robust modeling framework

The above two characteristics are both considered, and this Chapter proposes a data-driven PV generation uncertainty characterization method, shown as the below Fig. 5.12a. The general framework of the two-stage robust modeling is shown as Fig. 5.12b.

In Fig. 5.12a, owing to the high scalability and fast computational speed, the Extreme Learning Machine (ELM) is regarded as a useful learning technique for training a single hidden-stage feed-forward neural network [54]. In Fig. 5.12b, the forecasting values and error of irradiation density, wind speed, and temperature

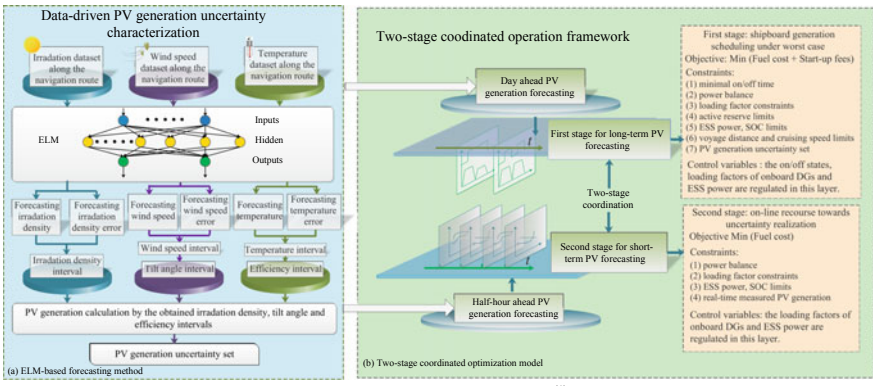

Fig. 5.12 Overall framework of proposed model. Reprinted from [52], with permission from IEEE

are obtained by ELM. Then three intervals, i.e., the irradiation density intervals $\left[I_{min,t}^{Gh}, I_{max,t}^{Gh}\right]$, the tilt angle intervals $\left[\phi_t^{min}, \phi_t^{max}\right]$ and the PV generation efficiency intervals $\left[\eta_{min,t}^{PV}, \eta_{max,t}^{PV}\right]$ are obtained by two different ways, i.e., $\left[I_{min,t}^{Gh}, I_{max,t}^{Gh}\right]$ is calculated by the forecasting values and error, and $\left[\phi_t^{min}, \phi_t^{max}\right]$, $\left[\eta_{min,t}^{PV}, \eta_{max,t}^{PV}\right]$ are calculated by the forecasting wind speed intervals and temperature intervals, since higher wind speed and temperature will lead to larger rolling effect and generation efficiency, respectively.

$$P_t^{PV} = \eta_t^{PV} \cdot A_{PV} \cdot I_t^{Gh} \cdot \begin{bmatrix} \cos\theta_t + C_{\phi_1}\left(\cos\frac{\phi_t}{2}\right)^2 \\ +C_{\phi_2}\left(\sin\frac{\phi_t}{2}\right)^2 \end{bmatrix} \tag{5.12}$$

Based on the obtained uncertain PV generation as (5.12), the proposed two-stage multi-timescale coordinated operation framework aims to coordinate different controllable resources in different timescales according to their different response characteristics considering the uncertain PV outputs, which is shown in Fig. 5.12b. In the day-ahead time-window, i.e., the first stage, the DGs' on/off states and the cruising speed, which cannot instantly respond to the uncertainties, are optimized based on day-ahead interval predictions of the PV generation. This stage aims to dispatch the DGs and ESS on a large time horizon to fulfill propulsion and service loads in the worst case of PV generation.

During the half-hour-ahead online operation time-window, i.e., the second stage, the loading factor of DGs and ESS are re-dispatched based on half-hour-ahead predictions of the PV generation. The half-hour-ahead predictions tend to be more accurate and they can be regarded as the uncertainty realization. Thus, the second-stage operation aims to compensate for the first-stage operation when the uncertainties realize in practice.

(3) Case description

In this study, a typical medium voltage direct current (MVDC) 4-DGs AES case is used to verify the proposed method. The topology and navigation data of this 4-DG AES are shown in Figs. 5.13 and 5.14, respectively. The topology is from [55], which follows the ABS-R2 standard [56]. In Fig. 5.13, 4 DGs are connected in two buses via AC/DC converters, and the circuit breaker is normally open. In general cases, two buses are located in different watertight compartments for avoiding operating risk. As for the PV generation uncertainty set characterization, the training datasets are also applied to [53], which are deduced from real-world navigation from Dalian, China to Aden, Yemen, and 2 MW PV modules are integrated into the AES for future applications. Other detailed parameters can be found in [52].

(4) Case study

To test the validity of the proposed forecasting process, three forecasting methods are compared. The results are shown in Fig. 5.15.

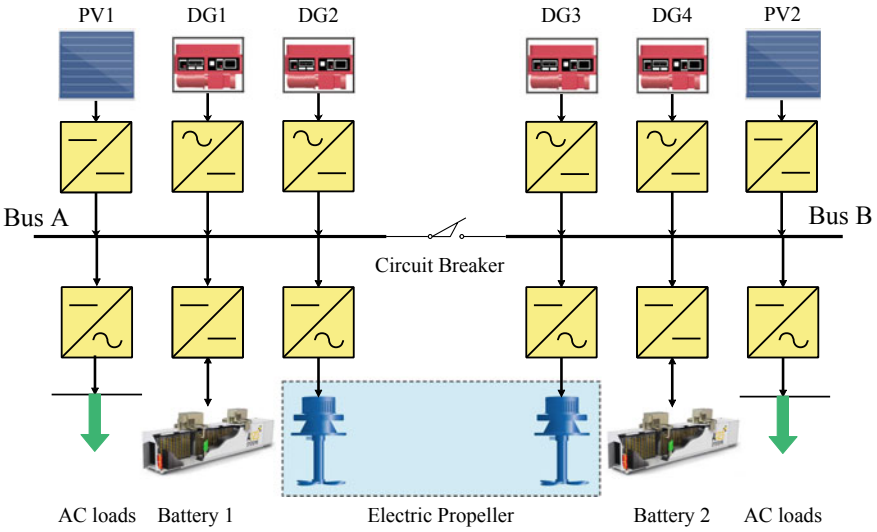

Fig. 5.13 Topology of 4-DG AES. Reprinted from [52], with permission from IEEE

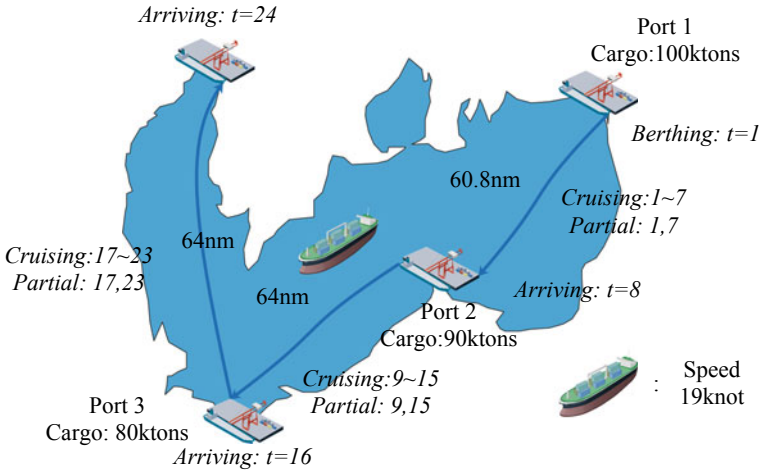

Fig. 5.14 Navigation scheme of AES. Reprinted from [53], with permission from IEEE

Forecasting method A: the proposed method considering both the movement and tilt angle (wind speed);

Forecasting method B: the proposed method without considering the tilt angle (wind speed);

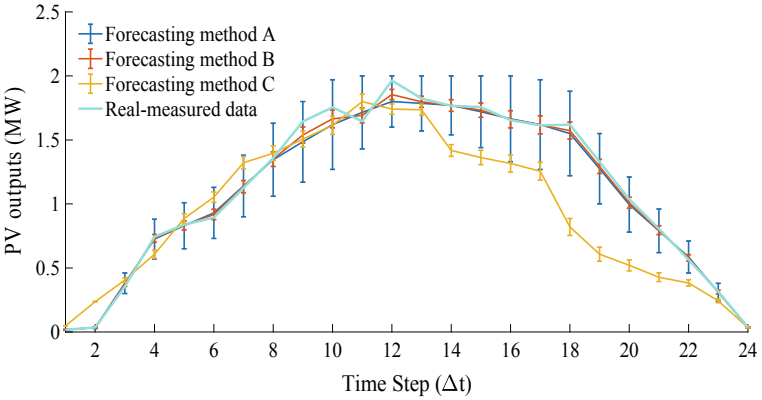

Fig. 5.15 Forecasting results under different methods. Reprinted from [53], with permission from IEEE

Forecasting method C: forecasting method only using the dataset in a stationary place (irradiation density, temperature) without considering the tilt angle.

From Fig. 5.15, the following conclusions can be found, (1) from the comparison between methods A and B, the forecasting intervals become much wider when considering tilt angle. This phenomenon suggests the rolling of the shipboard deck will bring more uncertainties to the PV generation, and if it is ignored, an optimistic scheme may be obtained; (2) from the comparison between method B and C, the forecast error of method C becomes rather large when the ship is away from the initial port ($t = 14 \sim 24$), which suggests the necessity to use the dataset along the navigation route to predict the PV generation.

The energy scheduling schemes in two stages are shown in Figs. 5.16 and 5.17, respectively. From Fig. 5.16, since the PV generations in the second stage are all larger than the worst case, the DGs' outputs are further replaced by the PV integration, which introduces further FC reductions. From Fig. 5.17, the ESS power in most of the partial intervals is increased, which means the PV generation increments are directly charged to the ESS in the partial intervals, therefore in the cruising intervals the ESS has more energy to shed the power demands of DGs than the first stage.

The above results manifest that, since the worst case of PV generation only happens in a small probability, therefore the single-stage robust method will introduce plenty of conservatism to the operating scheme, which leads to wastes on the PV generation. In this section, the online half-hour-ahead operation can effectively go against the uncertainty realization to improve the overall energy utilization efficiency while satisfying the constraints.

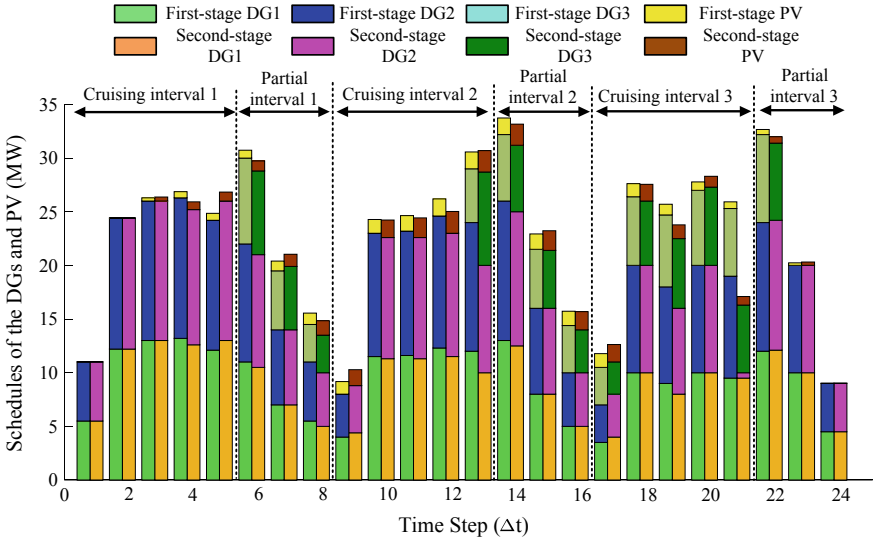

Fig. 5.16 Scheduling schemes of DGs in the first and second stages. Reprinted from [53], with permission from IEEE

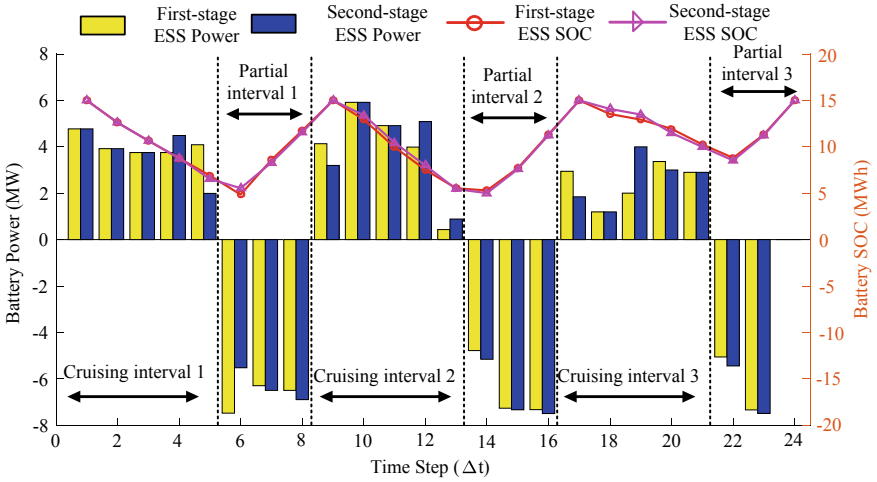

Fig. 5.17 ESS outputs and SOC in the first and second stages. Reprinted from [52], with permission from IEEE

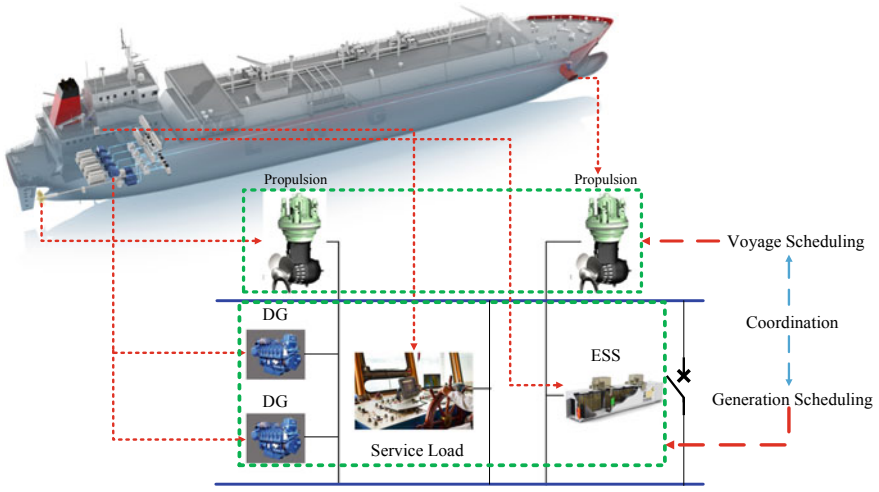

Fig. 5.18 Coordinated generation-voyage scheduling. Reprinted from [57], with permission from Elsevier

5.5.2 *Energy Management for Navigation Uncertainties in AES*

(1) Problem formulation

Besides the above PV power uncertainties, the navigation uncertainties are also commonly faced during the operation of AES. Fang and Xu [57] has studied this problem in detail, which is illustrated below. As shown in Fig. 5.18, the shipboard microgrid of an AES consists of DGs and ESS to meet the propulsion and service loads.

Compared with the conventional land-based microgrids, the AES (mobile microgrid) has the total voyage distance to the ports as a mandatory requirement, and therefore put extra constraints on the cruising speed of AES, as well as on the propulsion load. The generation scheduling aims to an economic energy scheme and the voyage scheduling aims to a punctual energy scheme. Both of them consist of a coordinated generation-voyage scheduling problem.

The speed loss when considering navigation uncertainties can be calculated by (5.1)–(5.4). The uncertainty set of the proposed model is formulated as following (4.13).

In this section, the wave height h, wavelength τ, weather direction angle θ and wind speed v^{wind} are four uncertain variables. In (4.13), $\overline{h_t}$, $\overline{\tau_t}$ and $\overline{v_t^{wind}}$ are the expectations of corresponding uncertain variables; $\underline{\mu}$ and $\bar{\mu}$ are the lower and upper budgets of the uncertainty set, when the lower budget falls and the upper budget rises, it means that the uncertainty set can cover higher uncertainty, leading to a higher robustness degree. Then the robust model shown in (5.6) is utilized to consider the worst influence by the navigation uncertainties.

$$\mathcal{U} = \left\{ \begin{array}{c} h_t \in \mathbb{R}^{|\mathcal{T}|} : h^{min} \le h_t \le h^{max}, \forall t \in \mathcal{T} \\ \underline{\mu^h} \le \sum_{t\in\mathcal{T}} h_t \Big/ \sum_{t\in\mathcal{T}} \overline{h_t} \le \overline{\mu^h} \\ \tau_t \in \mathbb{R}^{|\mathcal{T}|} : \tau^{min} \le \tau_t \le \tau^{max}, \forall t \in \mathcal{T} \\ \underline{\mu^\tau} \le \sum_{t\in\mathcal{T}} \tau_t \Big/ \sum_{t\in\mathcal{T}} \overline{\tau_t} \le \overline{\mu^\tau} \\ v_t^{wind} \in \mathbb{R}^{|\mathcal{T}|} : v_{min}^{wind} \le v_t^{wind} \le v_{max}^{wind} \\ \underline{\mu^v} \le \sum_{t\in\mathcal{T}} v_t^{wind} \Big/ \sum_{t\in\mathcal{T}} \overline{v_t^{wind}} \le \overline{\mu^v} \\ \vartheta \in \left[0, 180^o\right] : \theta_t = \varsigma \cdot \vartheta, \forall \varsigma \le 180/\vartheta \in \mathbb{N} \end{array} \right\} \tag{5.13}$$

(2) Case study

To test the effects of proposed robust model on the on-time rates, 500 water current scenarios are randomly sampled according to uniform distributions in each time-interval, denoted as $\left(h_{l,t}, \tau_{l,t}, v_{l,t}^{wind}\right)$, $t = 1 \sim 24$, $i = 1 \sim 500$. Robust 1 (The formulated robust model considering navigation uncertainties, abbreviated as R1) and Non-robust (conventional coordinated generation-voyage scheduling without navigation uncertainties, abbreviated as NR1) are set as operating strategies, respectively. The corresponding voyage distances of each sample at the scheduled time under $\theta = 30^o$ are shown in Fig. 5.19. The cruising speed and EEOI are shown in Fig. 5.20. The generation scheduling schemes are shown in Fig. 5.21. The worst speed loss and the corresponding on-time rates under different θ with or without wind are shown in Fig. 5.22.

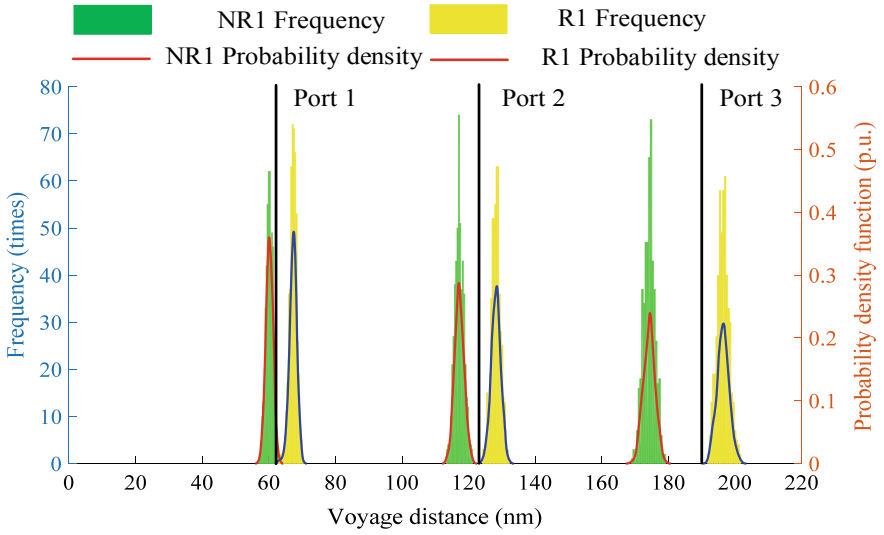

Fig. 5.19 On-time rates of different voyage schedules. Reprinted from [57], with permission from Elsevier

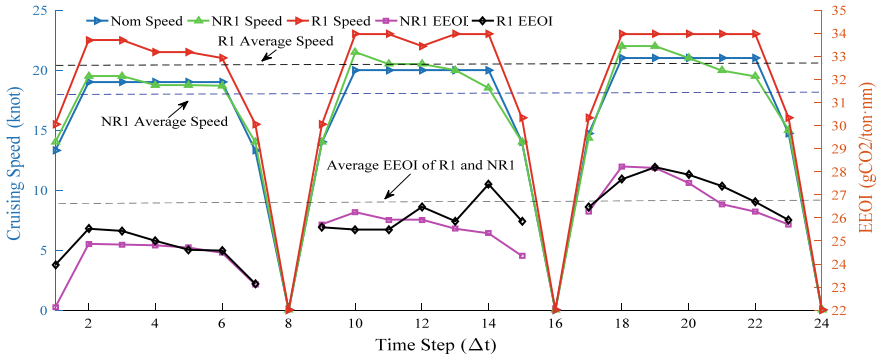

Fig. 5.20 Comparisons between NR1 and R1. Reprinted from [57], with permission from Elsevier

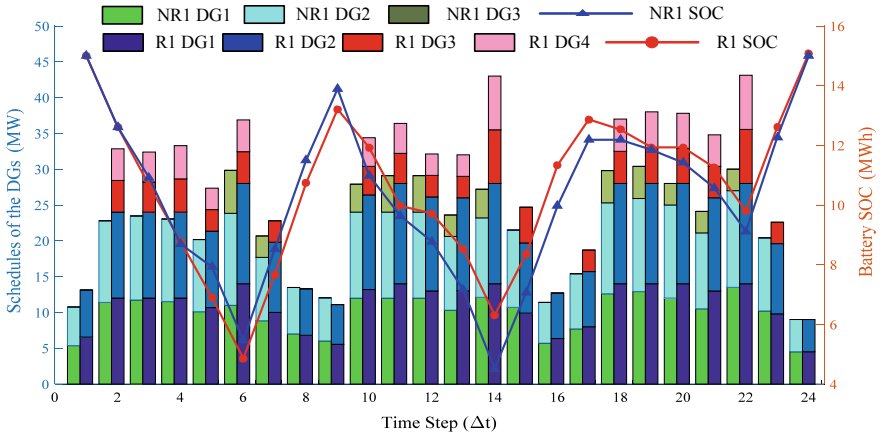

Fig. 5.21 Scheduling schemes of DGs and ESS of NR1 and R1. Reprinted from [57], with permission from Elsevier

Figure 5.19 clearly shows that the influences of uncertain water and wind will constantly accumulate during the voyage, which leads to an average 13 nm delay, leading to a 0% on-time rate of NR1 at the terminal port. However, the proposed robust model can accommodate these uncertainties by adjusting the outputs of the DGs and ESS. Accordingly, the corresponding on-time rates of R1 to each port are all 100%.

The reason to ensure the on-time rates of proposed method can be inferred from Figs. 5.20 and 5.21. The first berthing time-interval, $t = 0$, is not included in the analysis since the cruising speed and corresponding propulsion load are both zeros.

In Fig. 5.20, the cruising speed of robust model is higher than non-robust model, so able to cover the speed loss led by the wave and wind. Higher cruising speed suggests heavier propulsion load, so the corresponding outputs of DGs are all increased to meet the power demand increments, which leads to a higher FC. Specifically, in

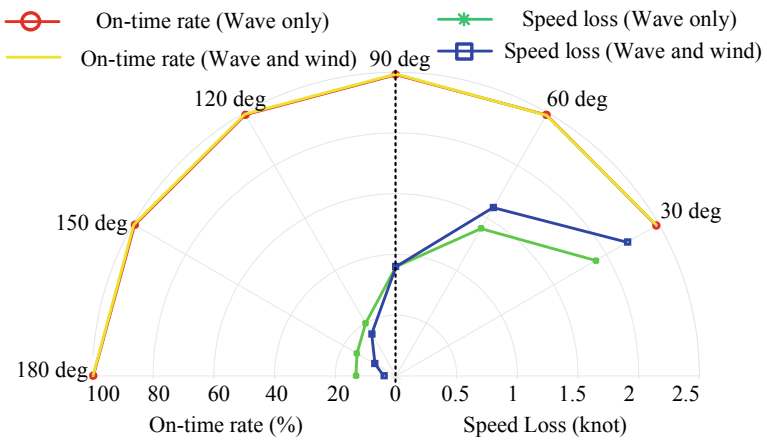

Fig. 5.22 Worst speed loss and corresponding on-time rates. Reprinted from [57], with permission from Elsevier

Fig. 5.21, NR1 uses no more than 3 DGs all the time, even 2 DGs in $t = 1 \sim 5, 8, 9, 15 \sim 17, 23, 24$. Correspondingly, R1 uses 4 DGs in most time during the voyage, only except the partial speed time-intervals, $t = 1, 7 \sim 9, 15 \sim 17, 23, 24$.

Figure 5.22 shows the worst speed loss and corresponding on-time rates. The yellow and red curves show that the proposed method can ensure a 100% on-time rate for all uncertain scenarios. The green curves show that the water wave always has negative impacts on the cruising speed, but the effect will gradually fade with the increment of the weather direction angle, which leads to the speed loss reductions.

Besides, it can be observed from Fig. 5.22 that, unlike water wave, the wind has quite different impacts on the speed loss in different scenarios, e.g. when $\theta \in [30°, 90°]$, the wind will increases speed loss, while when $\theta \in [90°, 180°]$, the wind can reduce speed loss. Especially when $\theta = 150°$ and $180°$, the speed loss under wave and wind are less than 0.5knot, thereby its negative impacts on the voyage scheduling can be greatly reduced. This is also the key reason for the cruising ships to choose their navigation route to the leeward side of wind.

References

1. Kim, M.: Estimation of added resistance and ship speed loss in a seaway. Ocean Eng. **141**, 465–476 (2017)
2. Harvald, S.A.: Resistance and propulsion of ships. Krieger Publishing Company, P.O. Box 9542, Melbourne, FL United States (1992)
3. Shao, W., Zhou, P., Thong, S.K.: Development of a novel forward dynamic programming method for weather routing. J. Mar. Sci. Technol. **17**(2), 239–251 (2012)
4. Padhy, C.P., Sen, D., Bhaskaran, P.K.: Application of wave model for weather routing of ships in the North Indian Ocean. Nat. Hazards **44**(3), 373–385 (2008)

5. Lin, Y.H., Fang, M.C., Yeung, R.W.: The optimization of ship weather-routing algorithm based on the composite influence of multi-dynamic elements. Appl. Ocean Res. **43**, 184–194 (2013)
6. Krata, P., Szlapczynska, J.: Ship weather routing optimization with dynamic constraints based on reliable synchronous roll prediction. Ocean Eng. **150**, 124–137 (2018)
7. Lai, K., Illindala, M.: Graph theory based shipboard power system expansion strategy for enhanced resilience. IEEE Trans. Ind. Appl. **54**(6), 5691–5699 (2018)
8. Xu, Q., Yang, B., Han, Q., et al.: Optimal power management for failure mode of MVDC microgrids in all-electric ships. IEEE Trans. Power Syst. **34**(2), 1054–1067 (2018)
9. Louit, D., Pascual, R., Banjevic, D., et al.: Optimization models for critical spare parts inventories—a reliability approach. J. Oper. Res. Soc. **62**(6), 992–1004 (2011)
10. Evans, P.M., Schultz, R.D.: Rotating electrical machine with electromagnetic and permanent magnet excitation. U.S. Patent 5,663,605. 1997-9-2
11. Sebille, D., Westerholt, E.: Control device for a reversible rotating electrical machine. U.S. Patent 7,102,304. 2006-9-5
12. Iris, Ç., Lam, J.S.: A review of energy efficiency in ports: Operational strategies, technologies and energy management systems. Renew. Sustain. Energy Rev. **112**, 170–182 (2019)
13. Jurong Port starts world's largest port-based solar facility. https://www.businesstimes.com.sg/energy-commodities/jurong-port-starts-worlds-largest-port-based-solar-facility
14. Man Diesel & Turbo, Basic principal of ship propulsion, 2012, Technical Report
15. Kim, M., Hizir, O., Turan, O., et al.: Estimation of added resistance and ship speed loss in a seaway. Ocean Eng. **141**, 465–476 (2017)
16. Sumalee, A., Uchida, K., Lam, W.: Stochastic multi-modal transport network under demand uncertainties and adverse weather condition. Transp. Res. Part C: Emerg. Technol. **19**(2), 338–350 (2011)
17. Sprenger, F., Maron, A., Delefortrie, G., et al.: Experimental studies on seakeeping and maneuverability of ships in adverse weather conditions. J. Ship Res. **61**(3), 131–152 (2017)
18. Hoven, V.: Power spectrum of horizontal wind speed in the frequency range from 0.0007 to 900 cycles per hour. J. Meteorol. **14**(2), 160–164 (1957)
19. Yao, J., Li, H., Liao, Y., et al.: An improved control strategy of limiting the DC-link voltage fluctuation for a doubly fed induction wind generator. IEEE Trans. Power Electron. **23**(3), 1205–1213 (2008)
20. Jiang, Q., Gong, Y., Wang, H.: A battery energy storage system dual-layer control strategy for mitigating wind farm fluctuations. IEEE Trans. Power Syst. **28**(3), 3263–3273 (2013)
21. Li, X., Hui, D., Lai, X.: Battery energy storage station (BESS)-based smoothing control of photovoltaic (PV) and wind power generation fluctuations. IEEE Trans. Sustain. Energy **4**(2), 464–473 (2013)
22. Kavasseri, R., Seetharaman, K.: Day-ahead wind speed forecasting using f-ARIMA models. Renew. Energy **34**(5), 1388–1393 (2009)
23. Li, G., Shi, J.: On comparing three artificial neural networks for wind speed forecasting. Appl. Energy **87**(7), 2313–2320 (2010)
24. Shi, J., Lee, W., Liu, Y., et al.: Forecasting power output of photovoltaic systems based on weather classification and support vector machines. IEEE Trans. Ind. Appl. **48**(3), 1064–1069 (2012)
25. Fernandez-Jimenez, L., Muñoz-Jimenez, A., Falces, A., et al.: Short-term power forecasting system for photovoltaic plants. Renew. Energy **44**, 311–317 (2012)
26. Li, J., Liu, Y., Wu, L.: Optimal operation for community-based multi-party microgrid in grid-connected and islanded modes. IEEE Trans. Smart Grid **9**(2), 756–765 (2016)
27. Kanellos, F.D., Volanis, E., Hatziargyriou, N.D.: Power management method for large ports with multi-agent systems. IEEE Trans. Smart Grid **10**(2), 1259–1268 (2017)
28. Moya, O.: A spinning reserve, load shedding, and economic dispatch solution by Bender's decomposition. IEEE Trans. Power Syst. **20**(1), 384–388 (2005)
29. Jaefari-Nokandi, M., Monsef, H.: Scheduling of spinning reserve considering customer choice on reliability. IEEE Trans. Power Syst. **24**(4), 1780–1789 (2009)

30. Banzo, M., Ramos, A.: Stochastic optimization model for electric power system planning of offshore wind farms. IEEE Trans. Power Syst. **26**(3), 1338–1348 (2010)
31. Abbey, C., Joós, G.: A stochastic optimization approach to rating of energy storage systems in wind-diesel isolated grids. IEEE Trans. Power Syst. **24**(1), 418–426 (2008)
32. Alqurashi, A., Etemadi, A., Khodaei, A.A.: Treatment of uncertainty for next generation power systems: State-of-the-art in stochastic optimization. Electric Power Syst. Res., **141**, 233–245 (2016)
33. Peng, C., Xie, P., Pan, L., et al.: Flexible robust optimization dispatch for hybrid wind/photovoltaic/hydro/thermal power system. IEEE Trans. Smart Grid **7**(2), 751–762 (2015)
34. Bertsimas, D., Litvinov, E., Sun, X., et al.: Adaptive robust optimization for the security constrained unit commitment problem. IEEE Trans. Power Syst. **28**(1), 52–63 (2012)
35. Minoux, M.: On robust maximum flow with polyhedral uncertainty sets. Optim. Lett. **3**(3), 367–376 (2009)
36. Ben-Tal, A., Nemirovski, A.: Robust solutions of uncertain linear programs. Oper. Res. Lett. **25**(1), 1–13 (1999)
37. Epanechnikov, V.: Non-parametric estimation of a multivariate probability density. Theory Probab. Appl. **14**(1), 153–158 (1969)
38. Xu, X., Yan, Z., Xu, S.: Estimating wind speed probability distribution by diffusion-based kernel density method. Electr. Power Syst. Res. **121**, 28–37 (2015)
39. Yuan, Y., Wang, J., Zhou, K., et al.: Monthly unit commitment model coordinated short-term scheduling and efficient solving method for renewable energy power system. Proc. CSEE **39**(18), 5336–5345 (2019)
40. Akhavan-hejazi, H., Mohsenian-rad, H.: Energy storage planning in active distribution grids: a chanceconstrained optimization with non-parametric probability functions. IEEE Trans. Smart Grid **9**(3), 1972–1985 (2016)
41. Kulkarni, V.: Modeling and Analysis of Stochastic Systems. CRC Press (2016)
42. Safta, C., Chen, R., Najm, H., et al.: Efficient uncertainty quantification in stochastic economic dispatch. IEEE Trans. Power Syst. **32**(4), 2535–2546 (2016)
43. Li, J., Ou, N., Lin, G., et al.: Compressive sensing based stochastic economic dispatch with high penetration renewables. IEEE Trans. Power Syst. **34**(2), 1438–1449 (2018)
44. Hu, Z., Xu, Y., Korkali, M., et al.: Uncertainty quantification in stochastic economic dispatch using Gaussian process emulation. 2020 IEEE Power & Energy Society Innovative Smart Grid Technologies Conference (ISGT), pp. 1–5. IEEE (2020)
45. Chen, Y., Wang, Y., Kirschen, D., et al.: Model-free renewable scenario generation using generative adversarial networks. IEEE Trans. Power Syst. **33**(3), 3265–3275 (2018)
46. Kong, W., Dong, Z., Jia, Y., et al.: Short-term residential load forecasting based on LSTM recurrent neural network. IEEE Trans. Smart Grid **10**(1), 841–851 (2017)
47. Hossain, M., Mekhilef, S., Danesh, M., et al.: Application of extreme learning machine for short term output power forecasting of three grid-connected PV systems. J. Clean. Prod. **167**, 395–405 (2017)
48. Li, P., Guan, X., Wu, J., et al.: Modeling dynamic spatial correlations of geographically distributed wind farms and constructing ellipsoidal uncertainty sets for optimization-based generation scheduling. IEEE Trans. Sustain. Energy **6**(4), 1594–1605 (2015)
49. Kumar, P., Yildirim, E.: Minimum-volume enclosing ellipsoids and core sets. J. Optim. Theory Appl. **126**(1), 1–21 (2005)
50. Ding, T., Lv, J., Bo, R., et al.: Lift-and-project MVEE based convex hull for robust SCED with wind power integration using historical data-driven modeling approach. Renew. Energy **92**, 415–427 (2016)
51. Velloso, A., Street, A., Pozo, D., et al.: Two-stage robust unit commitment for co-optimized electricity markets: An adaptive data-driven approach for scenario-based uncertainty sets. IEEE Trans. Sustain. Energy **11**(2), 958–969 (2019)
52. Fang, S., Xu, Y., Wen, S., et al.: Data-driven robust coordination of generation and demand-side in photovoltaic integrated all-electric ship microgrids. IEEE Trans. Power Syst. **35**(3), 1783–1795 (2019)

53. Wen, S., Lan, H., Hong, Y.Y., et al.: Allocation of ESS by interval optimization method considering impact of ship swinging on hybrid PV/diesel ship power system. Appl. Energy **175**, 158–167 (2016)
54. Wan, C., Lin, J., Song, Y., et al.: Probabilistic forecasting of photovoltaic generation: An efficient statistical approach. IEEE Trans. Power Syst. **32**(3), 2471–2472 (2016)
55. Kanellos, F.D., Tsekouras, G.J., Prousalidis, J.: Onboard DC grid employing smart grid technology: challenges, state of the art and future prospects. IET Electr. Syst. Transp. **5**(1), 1–11 (2014)
56. Patel, M.R.: Shipboard Electrical POWER Systems. CRC Press (2011)
57. Fang, S., Xu, Y.: Multi-objective robust energy management for all-electric shipboard microgrid under uncertain wind and wave. Int. J. Electr. Power Energy Syst. **117**, 105600 (2020)